Myelin-derived ephrinB3 restricts axonal regeneration and recovery after adult CNS injury

Philip Duffy[a], Xingxing Wang[a], Chad S. Siegel[a], Nathan Tu[a], Mark Henkemeyer[b], William B. J. Cafferty[a], and Stephen M. Strittmatter[a,1]

[a]Cellular Neuroscience, Neurodegeneration and Repair Program, Yale University School of Medicine, New Haven, CT 06536; and [b]Department of Developmental Biology, Kent Waldrep Center for Basic Research on Nerve Growth and Regeneration, University of Texas Southwestern Medical Center, Dallas, TX 75390

Edited by Joshua R. Sanes, Harvard University, Cambridge, MA, and approved February 16, 2012 (received for review August 25, 2011)

Recovery of neurological function after traumatic injury of the adult mammalian central nervous system is limited by lack of axonal growth. Myelin-derived inhibitors contribute to axonal growth restriction, with ephrinB3 being a developmentally important axonal guidance cue whose expression in mature oligodendrocytes suggests a role in regeneration. Here we explored the in vivo regeneration role of ephrinB3 using mice lacking a functional *ephrinB3* gene. We confirm that ephrinB3 accounts for a substantial portion of detergent-resistant myelin-derived inhibition in vitro. To assess in vivo regeneration, we crushed the optic nerve and examined retinal ganglion fibers extending past the crush site. Significantly increased axonal regeneration is detected in *ephrinB3*$^{-/-}$ mice. Studies of spinal cord injury in *ephrinB3*$^{-/-}$ mice must take into account altered spinal cord development and an abnormal hopping gait before injury. In a near-total thoracic transection model, *ephrinB3*$^{-/-}$ mice show greater spasticity than wild-type mice for 2 mo, with slightly greater hindlimb function at later time points, but no evidence for axonal regeneration. After a dorsal hemisection injury, increased corticospinal and raphespinal growth in the caudal spinal cord are detected by 6 wk. This increased axonal growth is accompanied by improved locomotor performance measured in the open field and by kinematic analysis. Thus, ephrinB3 contributes to myelin-derived axonal growth inhibition and limits recovery from adult CNS trauma.

neurology | locomotion

Adult mammalian central nervous system (CNS) neurons fail to regenerate to their targets after injury. Intensive research in recent decades has revealed that both the extracellular environment of the CNS and the intrinsic growth state of neurons determine the extent of axonal growth and repair after injury (1, 2). An inhibitory growth environment for axons has been attributed to products of glial cells, both oligodendrocytes and astrocytes. Myelin-derived inhibitors include Nogo-A (3, 4), myelin-associated glycoprotein (5, 6) (MAG), oligodendrocyte-associated glycoprotein (OMgp), repulsive guidance molecule (RGM) (7), semaphorins (8), and netrins (9). Activated astrocytes at the injury site proliferate to form a glial scar (10, 11) and enhance the deposition of inhibitory chondroitin sulfate proteoglycans (12–14).

It is striking that the majority of inhibitory molecules of the injured adult CNS are molecularly distinct from developmental axonal guidance cues, whether repellant or attractive (15). Eph-ephrin signaling has a known role in the regulation of axon guidance through contact repulsion, inducing neuronal growth cone collapse during the formation of sensory maps in the developing brain (16, 17). Members of this family are up-regulated following CNS injury (18, 19). EphA4 has been implicated in the response to injury both as an astrocyte and as a neuronally expressed protein, but its functional role in recovery from neuronal injury is not clear (20–23). Macrophage EphB3 has also been implicated in adult axon regeneration (24).

Of potential interest, ephrinB3 is known to be expressed by myelinating oligodendrocytes and to inhibit axonal extension (21). Additionally, ephrinB3 is known to function during development as a midline repellent for axons of the corticospinal tract in the spinal cord (17, 25, 26). The long fasciculated corticospinal tract develops normally in *ephrinB3*$^{-/-}$ mice, but segmental corticospinal tract (CST) projections cross the midline inappropriately after leaving the bundled dorsalCST, before reaching caudal synaptic targets. However, the abnormal bilateral synchronization of hindlimb gait observed in *ephrinB3*$^{-/-}$ mice does not depend on misrouted CST fibers but reflects excess midline crossing of EphA4-expressing segmental interneurons of the central locomotor pattern generator in the spinal cord (27–29).

The expression pattern of ephrinB3 in the adult is distinct from its pattern during development. Oligodendrocytes are the principal source of the protein in the mature CNS. The expression of ephrinB3 in midline palisade cells of the developing spinal cord is not detected in the adult. Moreover, Benson and colleagues have demonstrated that ephrinB3 is required for axonal growth inhibition by detergent-resistant fractions of CNS myelin in vitro (21). These data have suggested that ephrinB3 contributes to myelin-dependent failure of axonal regeneration, but this has not been tested in vivo. Here we examined axonal regeneration after CNS injury in *ephrinB3*$^{-/-}$ mice. We report significant axonal regeneration phenotype in this strain.

Results

***EphrinB3* Ablation Enhances Axonal Outgrowth on Detergent-Resistant Myelin Substrate.** First, we confirmed that ephrinB3 protein is enriched markedly in CNS myelin fractions (Fig. S1). To compare the relative roles of ephrinB3 and other molecules in contributing to myelin inhibition of neurite outgrowth, we cultured adult wild-type dorsal root ganglion (DRG) neurons on substrata coated with laminin plus buffer versus laminin plus myelin extracts. Both detergent-extractable and detergent-resistant myelin proteins were collected from *ephrinB3*$^{+/+}$, *ephrinB3*$^{-/-}$, and *nogo-ab(trap/trap)mag*$^{-/-}$*omgp*$^{-/-}$ (*NMO*$^{-/-}$) triple mutant brains and spinal cords. Dialyzed CHAPS-soluble myelin extract from *NMO*$^{-/-}$ mice is less inhibitory than that of *ephrinB3*$^{+/+}$ and *ephrinB3*$^{-/-}$ myelin (494 ± 22 μm versus 217 ± 44 μm and 205 ± 57 μm per neuron, respectively; Fig. S2), consistent with previous studies (21, 30). However, the CHAPS-insoluble extract from myelin of *ephrinB3*$^{-/-}$ mice is significantly less inhibitory than that from *ephrinB3*$^{+/+}$ or *NMO*$^{-/-}$ mice (522 ± 15 μm versus 442 ± 13 μm and 426 ± 45 μm per neuron, respectively; $P < 0.01$, ANOVA; Fig. S2). These results confirm the previous findings for the two

Author contributions: P.D., X.W., W.B.J.C., and S.M.S. designed research; P.D., X.W., C.S.S., and N.T. performed research; M.H. contributed new reagents/analytic tools; P.D., X.W., C.S.S., N.T., W.B.J.C., and S.M.S. analyzed data; and P.D., M.H., W.B.J.C., and S.M.S. wrote the paper.

The authors declare no conflict of interest.

This article is a PNAS Direct Submission.

[1]To whom correspondence should be addressed. E-mail: stephen.strittmatter@yale.edu.

This article contains supporting information online at www.pnas.org/lookup/suppl/doi:10.1073/pnas.1113953109/-/DCSupplemental.

biochemically distinct myelin fractions (21, 30) and suggest that ephrinB3 may contribute to myelin inhibition in vivo.

Optic Nerve Regeneration Is Enhanced in *ephrinB3*$^{-/-}$ Mice Following Crush Injury. Previous experiments have documented increased optic nerve regeneration following ablation or inhibition of signaling mediated by specific myelin-based inhibitory molecules such as NgR1 (31, 32). Here we investigated whether a similar phenomenon would be observed after ablation of *ephrinB3*. We performed an optic nerve crush in *ephrinB3*$^{+/+}$ and *ephrinB3*$^{-/-}$ mice and assessed optic nerve regeneration and retinal ganglion cell survival 2 wk after injury. Retinal ganglion cell axons were labeled anterogradely with cholera toxin β subunit (CTB) injection into the vitreous humor 3 d before sacrifice. There is little or no regeneration of CTB-positive *ephrinB3*$^{+/+}$ optic nerve axons (Fig. 1 *A*–*C*). In contrast, optic nerve fiber regeneration is detectable in *ephrinB3*$^{-/-}$ littermates (Fig. 1 *D*–*F* and *H*–*M*). Significantly greater regeneration is observed at 200, 500, and 1,000 μm central to the crush site in *ephrinB3*$^{-/-}$ mice ($P < 0.01$, compared with *ephrinB3*$^{+/+}$; Fig. 1*G*). Thus, endogenous ephrinB3 plays a role in limiting optic nerve regeneration in vivo.

We considered whether the increased numbers of regenerating axons might be derived indirectly from improved cell survival in mice lacking ephrinB3. Assessment of retinal ganglion cell survival 14 d after crush injury revealed 80% mortality for these neurons in both *ephrinB3*$^{+/+}$ (Fig. 1*O*) and *ephrinB3*$^{-/-}$ (Fig. 1*Q*) mice, consistent with the published wild-type literature (33, 34). Thus, the increased number of optic nerve axons in *ephrinB3*$^{-/-}$ mice after crush injury reflects a specific action of ephrinB3 in axonal regeneration.

Augmented Recovery of Locomotor Function in *ephrinB3*$^{-/-}$ Mice After Spinal Cord Injury. Given ephrinB3's contribution to myelin inhibition of axon growth in vitro (21) and optic nerve regeneration in vivo, we sought to determine whether functional recovery from spinal cord injury (SCI) might be greater in mice lacking ephrinB3. It has been reported that *ephrinB3*$^{-/-}$ mice exhibit a "hopping" movement during locomotion (17, 26, 27), so we performed detailed analysis of preinjury baseline stepping performance with high-speed video limb kinematics (32, 35). Markers placed over each joint of both hindlimbs were tracked pre- and postinjury during unassisted locomotion to provide the most functionally relevant performance. Uninjured *ephrinB3*$^{+/+}$ and *ephrinB3*$^{-/-}$ mice both exhibit robust step cycles (Fig. 2 *A*, *C*, and *D* and Fig. S3 *A* and *B*). There is no difference in foot swing from kinematics or stride length from footprint analysis between the two genotypes (Fig. S3 *C* and *D*). The *ephrinB3*$^{+/+}$ mice exhibit an alternating hindlimb gait as observed by overlaying right and left step cycles (Fig. S3*A*). In contrast, e*phrinB3*$^{-/-}$ mice exhibit overlapping of right and left foot gait cycles (Fig. S3*B*), consistent with previous reports (17, 26). *EphrinB3*$^{-/-}$ mice also exhibit significant deficits in preinjury rotorod performance

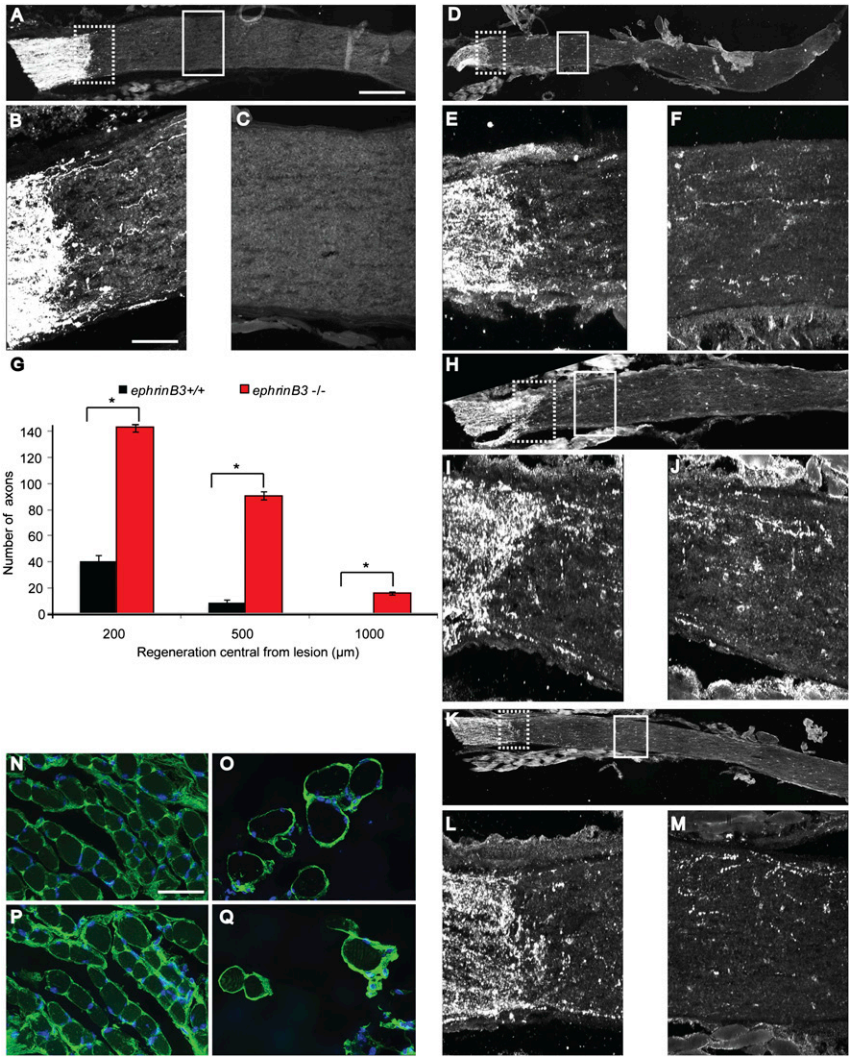

Fig. 1. Optic nerve regeneration is enhanced in *ephrinB3*$^{-/-}$ mice following crush injury. (*A*–*M*) Adult *ephrinB3*$^{+/+}$ and *ephrinB3*$^{-/-}$ mice underwent optic nerve crush, and the retinal ganglion cell axons were traced with CTB injection 2 wk after injury. Longitudinal optic nerve sections of *ephrinB3*$^{+/+}$ mice (*A*) show few CTB-immunoreactive regenerating fibers. Images from three separate *ephrinB3*$^{-/-}$ mice (*D*, *H*, and *K*) show axons passing through the crush site into the distal optic nerve. Higher-magnification views of the crush site are provided in *B*, *E*, *I*, and *L* (corresponding to dashed boxes in *A*, *D*, *H*, and *K*, respectively) and of the distal nerve in *C*, *F*, *J*, and *M* (corresponding to dashed boxes in *A*, *D*, *H*, and *K*, respectively). (*G*) The number of regenerating axons per optic nerve was measured from sections as in *A*–*M* as a function of distance from the crush site. Data are mean ± SEM for $n = 8$ mice per genotype; $^*P < 0.01$, Student's two-way *t* test. (*N*–*Q*) Retinal ganglion cell density was detected by anti–Thy-1 antibody staining of retinas. Images are from uninjured (*N* and *P*) and 17 d postinjury (*O* and *Q*) mice of *ephrinB3*$^{+/+}$ (*N* and *O*) and *ephrinB3*$^{-/-}$ (*P* and *Q*) genotypes. Ganglion cell loss after injury was ~80% in both genotypes. [Scale bars, 200 μm (*A* and *H*), 300 μm (*D* and *K*), and 50 μm (*B*, *C*, *E*, *F*, *I*, *J*, *L*, and *M*).]

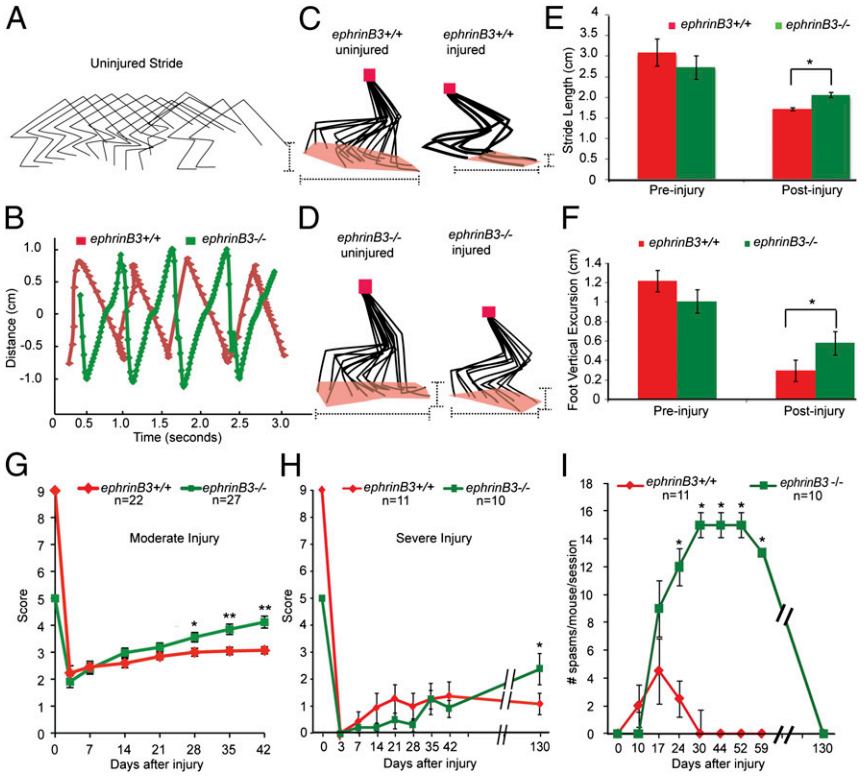

Fig. 2. *EphrinB3*$^{-/-}$ mice exhibit greater functional recovery after moderate and severe thoracic spinal cord injury. *EphrinB3*$^{+/+}$ and *ephrinB3*$^{-/-}$ littermate mice were examined before or at various times after midthoracic spinal cord injuries of moderate (dorsal hemisection; *B*–*G*) or severe (near-total transection; *H* and *I*) intensity. (*A*) Tracings of joint and limb position from one side of a wild-type uninjured mouse during one gait cycle are shown for every 21st frame of the video. The mouse is moving to the right. (*B*) At 5–6 wk after moderate SCI, video kinematic analysis of hindlimb movement was obtained as in *A*. The anterior–posterior position of the foot relative to the hip from one limb of *ephrinB3*$^{+/+}$ and *ephrinB3*$^{-/-}$ mice is plotted as a function of time. Gait cycles are reflected in sequential peaks. Note that the excursion of the *ephrinB3*$^{-/-}$ mouse is greater than that of the wild-type mouse. (*C* and *D*) Foot, ankle, and knees have been normalized to the hip position (red squares) from kinematic analysis as in *A*, obtained before and 5–6 wk after moderate spinal cord injury for an *ephrinB3*$^{+/+}$ (*C*) and *ephrinB3*$^{-/-}$ (*D*) mouse. The extents of foot swing and excursion are highlighted (dotted lines) and are greater in the postinjury *ephrinB3*$^{-/-}$ mouse. (*E* and *F*) The stride length (*E*) and foot vertical excursion (*F*) relative to the hip were measured as in *C* and *D* and are reported as mean ± SEM, $n = 26$ limbs for *ephrinB3*$^{+/+}$ and $n = 22$ for *ephrinB3*$^{-/-}$. $^{*}P < 0.01$, one-way ANOVA. (*G* and *H*) BMS scores for moderate (*G*) and severe (*H*) injury in *ephrinB3*$^{+/+}$ and *ephrinB3*$^{-/-}$ mice. *EphrinB3*$^{-/-}$ mice recover to a greater extent in both lesion severities. $^{*}P < 0.01$, $^{**}P < 0.002$, one-way ANOVA. (*I*) The number of extensor hindlimb spasms per mouse per observation period is plotted for the severe-injury group. $^{*}P < 0.01$, one-way ANOVA.

(Fig. S3*E*), in stride-width footprint analysis (Fig. S3*F*), and in baseline Basso Mouse Scale (BMS) locomotor scores (Fig. 2 *G* and *H*). These data demonstrate that motor performance of *ephrinB3*$^{-/-}$ mice is impaired before injury.

Two severities of spinal cord injury were created in the midthoracic spinal cord of 2- to 4-mo-old mice: a dorsal hemisection (moderate injury) and a near-total transection (severe injury). Behavioral outcomes were assessed during the period 0–25 wk after injury and anatomical outcomes after subsequent axonal tracing and sacrifice. Six hours after midthoracic spinal cord injury, all mice displayed flaccid hindlimb paralysis and regained some function over the observation period.

For the control *ephrinB3*$^{+/+}$ group, unassisted gait metrics remained significantly impaired 5–6 wk after moderate dorsal hemisection (Fig. 2*C*). We focused on kinematic measures of the length and height of foot swing with each step cycle for dorsal hemisection mice, metrics that were equivalent in preinjury *ephrinB3*$^{+/+}$ and *ephrinB3*$^{-/-}$ mice. The anterior–posterior length of the foot swing relative to the hip in *ephrinB3*$^{+/+}$ mice (stride length) was reduced by 50% following injury (3.1 ± 0.3 cm versus 1.6 ± 0.1 cm; Fig. 2 *C* and *E*). The vertical excursion of the foot cycle relative to the hip was reduced by 75% (1.2 ± 0.1 cm versus 0.3 ± 0.133 cm; Fig. 2 *C* and *F*).

The recovery of hindlimb movement in *ephrinB3*$^{-/-}$ mice after moderate injury was markedly greater than that observed in wild-type littermates (Fig. 2 *B* and *D*–*F*). The stride length was reduced by only 20% compared with preinjury values (2.7 ± 0.3 cm versus 2.1 ± 0.1 cm; Fig. 2 *D* and *E*) and vertical foot excursion by only 40% (1.0 ± 0.1 cm versus 0.6 ± 0.1 cm; Fig. 2 *D* and *F*). Postinjury hindlimb foot movements relative to the hip were greater for *ephrinB3*$^{-/-}$ than control littermate mice in both the anterior–posterior and vertical dimensions ($P < 0.05$, ANOVA; Fig. 2 *E* and *F*).

The increased post–moderate-injury limb movement of *ephrinB3*$^{-/-}$ mice was reflected in greater recovery of open-field locomotor BMS scores (Fig. 2*G*). Wild-type mice initially exhibited full-scale BMS scores of 9 and reached a level of 3.1 ± 0.1 at 6 wk postinjury, whereas *ephrinB3*$^{-/-}$ mice started with BMS scores of 5 but recovered to values of 4.1 ± 0.2 ($P < 0.005$, one-way ANOVA; Fig. 2*G*).

We assessed the robustness of the *ephrinB3*$^{-/-}$ phenotype by analyzing a more severe injury (Fig. 2 *H* and *I*). With a near-total midthoracic transection, recovery as measured by BMS score is limited regardless of genotype. For control mice, BMS scores remained at 1.1 ± 0.4, reflecting minimal hindlimb movements even 4 mo after injury (Fig. 2*H*). The *ephrinB3*$^{-/-}$ cohort had BMS scores indistinguishable from the control group between 0 and 2 mo after injury, but behaved with a dramatically different phenotype in the open field. Movement-induced bilateral extensor spasms of the hindlimbs were frequent in the mice lacking ephrinB3 between 2 and 9 wk after injury (Fig. 2*I* and Movie S1). Such spasms were rarely observed between 1 and 3 wk postinjury in wild-type mice with severe thoracic lesions and were completely absent thereafter.

With recovery times of greater than 4 mo, extensor spasms in the *ephrinB3*$^{-/-}$ severe-injury mice resolved (Fig. 2*I*). At this time point, the open-field locomotor BMS scores demonstrate a significant improvement in the *ephrinB3*$^{-/-}$ group to 2.4 ± 0.6 ($P < 0.05$ relative to control; Fig. 2*H*). Thus, recovery of *ephrinB3*$^{-/-}$ mice from severe thoracic spinal cord injury is complicated by extensor spasms in the subacute phase, but eventually reaches better performance than control mice.

CST Regeneration After Dorsal Hemisection in *ephrinB3*$^{-/-}$ Mice. The optic nerve and in vitro data suggest that increased functional recovery after spinal cord trauma in *ephrinB3*$^{-/-}$ mice is due to injury-induced axonal growth, so we attempted to correlate functional recovery seen in behavioral tests with regeneration of anatomical tracts. The CST is a vital pathway for fine motor function in humans. The mouse dorsal hemisection lesion severs

the main CST running in the ventral portion of the dorsal columns, as well as the minor, but functionally significant, component running in the lateral funiculi, while sparing extremely rare uncrossed ventral fibers. Therefore, we examined the CST projection pattern in *ephrinB3*$^{+/+}$ and *ephrinB3*$^{-/-}$ mice by anterograde biotin dextran amine (BDA) tracing 6 wk after bilateral dorsal hemisection lesions of the midthoracic spinal cord.

CST axons are seen approaching the lesion site in *ephrinB3*$^{+/+}$ mice (Fig. 3 *A* and *B*) but not do penetrate or traverse the lesion site caudally (Fig. 3*C*). *EphrinB3*$^{-/-}$ mice exhibit large numbers of BDA-positive CST axons entering the lesion site (Fig. 3 *D*, *H*, *I*, *K*, *L*, *N*, and *O*; examples from four mice). A number of these fibers extend into the caudal spinal cord of the *ephrinB3*$^{-/-}$ mice (Fig. 3 *E*, *J*, *M*, and *P*). In dual-label immunohistochemistry with anti-SV2, CST fibers have morphological characteristics consistent with synaptic connections to caudal interneurons (Fig. 3 *E* and *F*).

Quantification of the number of CST axons present at 2 and 1 mm proximal and 100, 200, and 300 μm distal to the lesion site reveals significantly greater numbers of axons in the *ephrinB3*$^{-/-}$ mice (Fig. 3*Q*; $P < 0.01$, ANOVA). Whereas CST regeneration was detected in the *ephrinB3*$^{-/-}$ moderate-injury group, no CST fibers extended to the injury site in the *ephrinB3*$^{-/-}$ severe near-total transection group (0 ± 0 axons at the lesion center, mean ± SEM, $n = 6$ severe-injury *ephrinB3*$^{-/-}$ mice).

The presence of caudal CST fibers in the *ephrinB3*$^{-/-}$ moderate-injury group suggests either regenerative growth, fiber sparing, or distal sprouting. To separate these possibilities, we examined another cohort of mice, injected with BDA at the time of injury and killed 10 d postinjury (Fig. 3*Q*). CST analysis of *ephrinB3*$^{-/-}$ mice at this time point demonstrates axon retraction from the lesion site and no caudal fibers (Fig. 3*Q*, black line). Thus, the fibers in the lesion site and caudal to the lesion at 42 d postinjury reflect regenerative growth after moderate injury.

The expression of ephrinB3 in mature oligodendrocytes and the diminished inhibitory activity of *ephrinB3*$^{-/-}$ detergent-resistant myelin suggest that reduced environmental inhibition is the basis of CST regeneration. An alternative explanation is an altered degree of tissue loss and traumatic reaction. We assessed tissue sparing and GFAP immunoreactivity in the spinal cords of injured mice (Fig. 3 *R–T*). The moderate injury spared nearly half of spinal cord tissue (Fig. 3*R*), whereas only 15% of tissue was intact after severe injury (Fig. 3*S*). The *ephrinB3* genotype did not alter tissue sparing (Fig. 3*T*), indicating that CST regeneration and improved functional recovery is not secondary to a role of *ephrinB3* in tissue reaction or cell survival.

Increased Raphespinal Axon Length in the Caudal Spinal Cord of Injured *ephrinB3*$^{-/-}$ Mice. The dorsal hemisection injury model damages multiple descending spinal tracts in addition to the CST, including the serotonergic raphespinal tract (RST). The RST contributes significantly to locomotion in rodents (36, 37), and can be examined histologically with an anti–5-hydroxytryptamine (5HT) antibody. We focused our analysis on the ventral horn of the lumbar spinal cord (Fig. 4 *A* and *B*), where the RST is known to synapse on motor neurons (38). Raphespinal

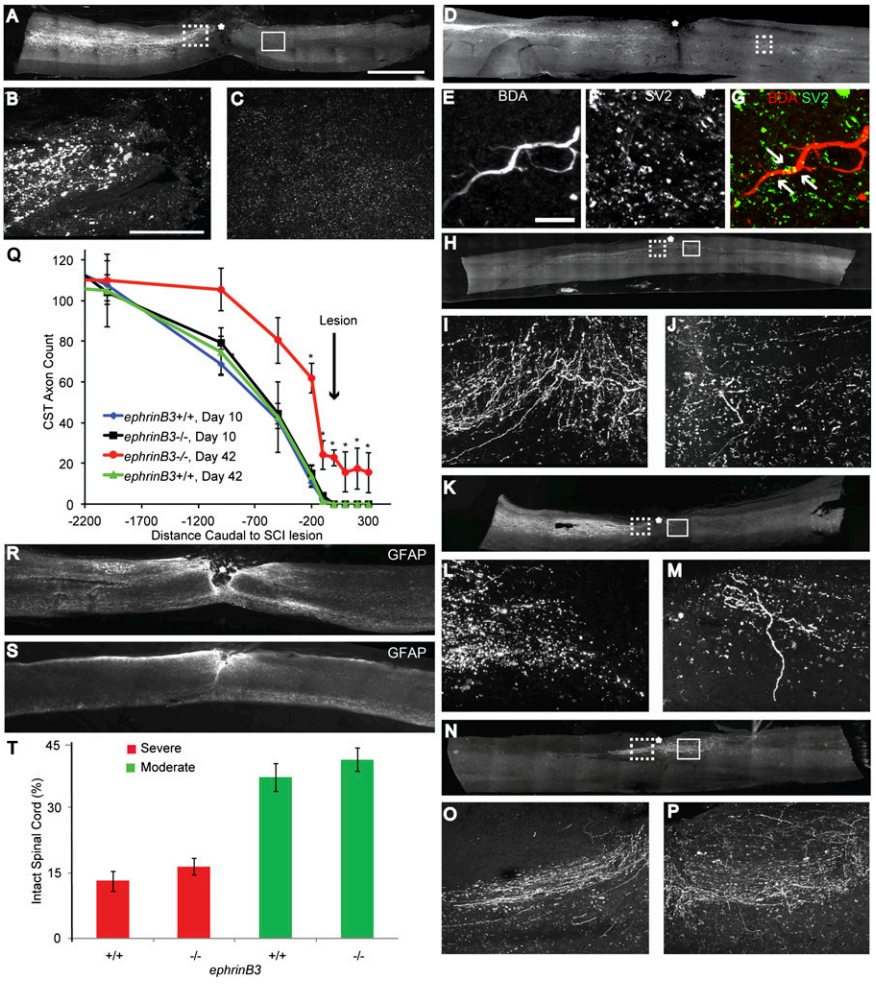

Fig. 3. Corticospinal axon regeneration after dorsal hemisection injury in *ephrinB3*$^{-/-}$ mice. (*A–F* and *H–P*) Adult *ephrinB3*$^{+/+}$ and *ephrinB3*$^{-/-}$ mice underwent moderate dorsal hemisection of the midthoracic spinal cord. Four weeks after injury, the CST was traced by cortical BDA injection before sacrifice at 6 wk after injury. Photomicrographs illustrate BDA-immunoreactive CST axons in sagittal sections of one *ephrinB3*$^{+/+}$ (*A–C*) and four *ephrinB3*$^{-/-}$ (*D–P*) mice. Dorsal is up and caudal is right. High-magnification views immediately rostral to the injury site (*B*, *I*, *L*, and *O*, corresponding to dotted boxes in *A*, *H*, *K*, and *N*) illustrate that CST fibers stop short of the lesion (asterisks) in wild-type mice (*B*) but extend further in *ephrinB3*$^{-/-}$ mice (*D*, *I*, *L*, and *O*). High-magnification views caudal to the injury site (*C*, *E*, *J*, *M*, and *P*, corresponding to solid boxes in *A*, *H*, *K*, and *N* or the dotted box in *D*) illustrate CST fibers extending past the lesion site only in *ephrinB3*$^{-/-}$ mice (*E*, *J*, *M*, and *P*). A double stain of caudal BDA fibers in *ephrinB3*$^{-/-}$ mice (*E*; red in *G*) with anti-SV2 (*F*; green in *G*) reveals overlap of the synaptic marker with CST fibers (arrows in *G*). [Scale bars, 2 mm (*A*, *D*, *H*, *K*, and *N*), 20 μm (*E–G*), and 100 μm (*B*, *C*, *I*, *J*, *L*, *M*, *O*, and *P*).] (*Q*) The number of CST axons is reported as a function of rostral–caudal distance from the injury site from sections as in *A–P* from mice 42 d postinjury. A separate cohort of dorsal hemisection mice were injected with BDA at the time of injury and killed 10 d postinjury. Data are mean ± SEM for $n = 8$–10 mice per genotype at day 42 and $n = 6$ per genotype at day 10. *$P < 0.05$, one-way ANOVA after LSD post hoc pairwise comparisons for *ephrinB3*$^{-/-}$, day 42 versus *ephrinB3*$^{+/+}$, day 42. (*R* and *S*) Spared tissue at the injury site was assessed after anti-GFAP staining of sagittal sections for severe near-total transection (*R*) and moderate dorsal hemisection (*S*). (*T*) The extent of spared tissue at the injury site was quantified from sections as in *R* and *S* as a functional of genotype. No statistical difference between genotypes was detected. Data are mean ± SEM for separate mice.

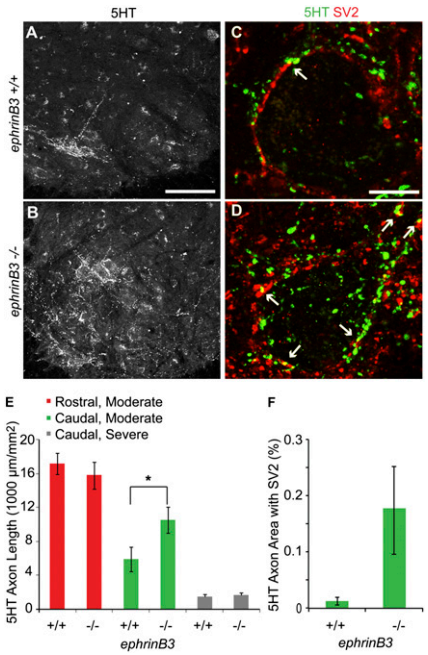

Fig. 4. *EphrinB3*$^{-/-}$ raphespinal fiber length is increased caudal to a hemisection of moderate severity. (*A* and *B*) Photomicrographs of 5HT-immunoreactive raphespinal fibers in a transverse section of the ventral horn of the lumbar spinal cord. Sections are from *ephrinB3*$^{+/+}$ and *ephrinB3*$^{-/-}$ mice at 42 d after a moderate dorsal hemisection injury. Dorsal is up and medial is right. (Scale bar, 75 µm.) (*C* and *D*) Confocal images of double immunohistology for 5HT (green) and SV2 (red) at high magnification from the ventral horn are shown. Colocalization of markers is indicated (arrows). (Scale bar, 15 µm.) (*E*) Raphespinal tract fiber lengths are measured from images as in *A* and *B* for the indicated genotypes, lesion severities, and spinal cord levels. Caudal to a lesion of moderate severity, *ephrinB3*$^{-/-}$ animals exhibit significantly greater fiber length compared with *ephrinB3*$^{+/+}$ mice. $*P < 0.05$, one-way ANOVA. Data are mean ± SEM for separate mice. (*F*) The fraction of 5HT-immunoreactive pixels also immunoreactive for SV2 as in *C* and *D* is measured. Data are mean ± SEM for separate mice.

anatomy was examined at 6 wk after moderate injury or 25 wk after severe injury. Rostral to the lesion, 5HT immunolabeling shows that raphespinal fiber length in the ventral horn is not significantly different between genotypes (Fig. 4*E*). Raphespinal fiber length is decreased in both *ephrinB3*$^{+/+}$ and *ephrinB3*$^{-/-}$ mice caudal to the injury (Fig. 4 *A*, *B*, and *E*). However, *ephrinB3*$^{-/-}$ mice at 42 d after dorsal hemisection injury exhibit significantly greater fiber length than *ephrinB3*$^{+/+}$ controls (Fig. 4 *B* and *E*; $P < 0.05$, ANOVA). With severe near-total transection, RST axon length was low in the lumbar ventral horn of both genotypes (Fig. 4*E*). Because the RST is not fully lost after dorsal hemisection injury in *ephrinB3*$^{+/+}$ mice, the increased fiber density may be due to increased growth of 5HT fiber in the caudal spinal cord, as opposed to regenerative growth across the lesion site.

The colocalization of immunoreactivity for the synaptic marker SV2 in caudal 5HT fibers was assessed as an indication of serotonergic synapses in the moderate hemisection group (yellow in Fig. 4 *C* and *D*). Confocal analysis demonstrates greater colocalization of SV2 and 5HT in the caudal ventral horn of *ephrinB3*$^{-/-}$ mice (Fig. 4*F*). This finding is consistent with synapse reformation after fiber sprouting in *ephrinB3*$^{-/-}$ mice.

Discussion

The main conclusion from this study is that ephrinB3 plays a role in limiting anatomical regeneration and functional recovery after adult mammalian CNS injury. Deletion of *ephrinB3* reduces the inhibitory activity of CNS myelin to neurite outgrowth of DRG cells in vitro. This phenomenon is associated with an in vivo regeneration phenotype after either optic nerve crush or dorsal hemisection of the thoracic spinal cord. Functional recovery after spinal cord injury without ephrinB3 is complicated by baseline motor impairment in *ephrinB3*$^{-/-}$ mice, and includes elevated extensor spasms after severe spinal cord injury. However, with moderate injury, hindlimb movements and gait assessment in the open field are significantly better in ephrinB3-null mice than in wild-type mice. We conclude that ephrinB3 is a physiologically important myelin-associated inhibitor of axonal growth in the adult central nervous system.

Detergent-resistant fractions of myelin extracted from ephrinB3-null mice are less inhibitory to DRG neurite outgrowth in vitro than wild-type myelin. These findings confirm a previous study undertaken by Benson and colleagues that showed that ephrinB3 is a potent inhibitor of neurite outgrowth (21). Whereas inhibition by the detergent-resistant fraction depends largely on ephrinB3 for inhibition, the detergent-soluble fraction of myelin depends primarily on the combination of Nogo, MAG, and OMgp (30). Spinal cord injury studies with *ephrinB3*$^{-/-}$ mice here, in combination with previous studies with Nogo, MAG, OMgp triple knockout mice (30), suggest that all four proteins contribute to in vivo limitation of axonal growth after CNS trauma by myelin. The greatest degree of regeneration and recovery may be achieved through combined interruption of ephrinB3 and NgR1 ligands.

Antagonizing myelin-based inhibitor signaling has previously shown efficacy in regenerating optic nerve axons following crush injury (31, 32, 39, 40). Here we find that deleting ephrinB3 expression has a similar effect on optic nerve axon regeneration. Optic nerve regeneration following crush injury in *ephrinB3*$^{-/-}$ mice is significantly greater than in *ephrinB3*$^{+/+}$ littermates at distances up to 1,000 µm distal to the crush site.

EphrinB3 and its receptor EphA4 are expressed by optic nerve oligodendrocytes and optic nerve axons, respectively (41–43). Ablation of ephrinB3-mediated signaling presumably allows EphA4-expressing optic nerve axons to regenerate past the region of the crush site. The extent of regeneration quantified as the number of regenerating axons is approximately sevenfold less than that observed following optic nerve crush in an *ngr1*$^{-/-}$ mouse at similar distances from the injury site (32). This difference in regenerative phenotype between mutant strains is likely the result of continued inhibitory signaling through the NgR1 in the *ephrinB3*$^{-/-}$ strain. A synergistic effect of removal of both NgR1-mediated and ephrinB3-induced inhibitory signaling on optic nerve regeneration is currently being investigated through the generation of *ngr1*, *ephrinB3* double mutant mice.

We observed regeneration of CST axons past the lesion site plus growth of RST axons in the caudal spinal cord after moderate dorsal hemisection in *ephrinB3*$^{-/-}$ mice (Figs. 3 and 4). This finding provides a correlation with improved hindlimb kinematic analysis metrics after injury, and suggests that enhanced growth of these two pathways contributes to the recovery process. However, the growth of multiple fiber systems exposed to myelin in local and long-distance circuits both rostral and caudal to the injury site is likely to play a role. Increased CST and RST growth were not observed following a severe near-total transection injury, despite functional recovery in the open field after both lesions. Thus, the late recovery of severely injured mice must be due to alternative fiber systems and neuroanatomical sites. This is consistent with the hypothesis that multiple pathways relevant to functional recovery are sensitive to inhibition by myelin and ephrinB3. Frank axon regeneration of long-tract descending pathways is only one of several mechanisms contributing to improved neurological function after moderate SCI in the absence of ephrinB3.

The gait-induced hindlimb extensor spasm phenotype of severely injured *ephrinB3*$^{-/-}$ mice is prominent during the period 1–2 mo after injury and limits locomotor performance. Extensor spasms are known to be debilitating clinical complications of

SCI requiring pharmacological and/or surgical intervention. In the case of *ephrinB3*$^{-/-}$ mice, the spasms resolve after several weeks. The basis for these injury-induced spasms is not likely to be simple. On the one hand, increased rearrangement of caudal circuitry released by injury in the absence of myelin-derived ephrinB3 may support these spasms. In this regard, excessive axon growth after injury may be deleterious for function. Not mutually exclusive, developmental abnormalities of interneuron projections in the *ephrinB3*$^{-/-}$ spinal cord that are responsible for the loss of alternating hindlimb movements (17, 27) may interact with injury-induced changes to support spasms. Further study of this model may delineate the pathophysiology of spontaneous extensor spasms associated with spinal cord injury.

The data demonstrate that ephrinB3 has a role as a myelin-based inhibitory protein in CNS repair, and that it may function in parallel or synergistically with Nogo, MAG, and OMgp. However, given its function as a developmental guidance cue and the observed extensor spasm phenotype of ephrinB3 mutant mice, it seems extremely likely that recovery mediated by inhibition of ephrinB3 signaling is not simply limited to altered myelin-based neurite outgrowth inhibition. The creation of a cell type-specific and temporally drug-regulated conditional deletion of the *ephrinB3* gene will be critical to further define the role of ephrinB3 as an inhibitory mediator of CNS regeneration.

Materials and Methods

Neurite Outgrowth. Adult dorsal root ganglion neurons were cultured and analyzed for outgrowth in the presence or absence of myelin fractions, as described (30, 44).

Optic Nerve Injury and CTB Tracing. The optic nerve was crushed 1 mm retroorbitally with forceps, and retinal ganglion cell axon regeneration was analyzed by anterograde CTB tracing at 14 d after crush (31, 32).

Spinal Cord Injury. Mouse thoracic spine level T6 spinal cord injury was achieved in *ephrinB3*$^{-/-}$ and *ephrinB3*$^{+/+}$ littermates after dorsal laminectomy (30, 37, 44, 45). Either dorsal hemisection or near-total transection was performed. Mice were observed for spontaneous extensor spasms and locomotion using the BMS scale. Video analysis of limb kinematics has been described for rats (32). CST axons were traced with BDA, and RST axons were immunostained (30, 44).

All animal procedures were reviewed and approved by the Yale Animal Care and Use Committee. Detailed methods are provided in *SI Materials and Methods*.

ACKNOWLEDGMENTS. We thank Noam Harel for advice regarding Simi video gait kinematics. This work was supported by grants from The Christopher and Dana Reeve Foundation, the Wings for Life Foundation, The Dr. Ralph and Marion Falk Medical Research Trust, and the National Institutes of Health (to M.H., W.B.J.C., and S.M.S.).

1. Akbik F, Cafferty WB, Strittmatter SM (June 15, 2011) Myelin associated inhibitors: A link between injury-induced and experience-dependent plasticity. *Exp Neurol*, 10.1016/j.expneurol.2011.06.006.
2. Liu BP, Cafferty WB, Budel SO, Strittmatter SM (2006) Extracellular regulators of axonal growth in the adult central nervous system. *Philos Trans R Soc Lond B Biol Sci* 361:1593–1610.
3. Chen MS, et al. (2000) Nogo-A is a myelin-associated neurite outgrowth inhibitor and an antigen for monoclonal antibody IN-1. *Nature* 403:434–439.
4. GrandPré T, Nakamura F, Vartanian T, Strittmatter SM (2000) Identification of the Nogo inhibitor of axon regeneration as a Reticulon protein. *Nature* 403:439–444.
5. McKerracher L, et al. (1994) Identification of myelin-associated glycoprotein as a major myelin-derived inhibitor of neurite growth. *Neuron* 13:805–811.
6. Mukhopadhyay G, Doherty P, Walsh FS, Crocker PR, Filbin MT (1994) A novel role for myelin-associated glycoprotein as an inhibitor of axonal regeneration. *Neuron* 13:757–767.
7. Hata K, et al. (2006) RGMa inhibition promotes axonal growth and recovery after spinal cord injury. *J Cell Biol* 173(1):47–58.
8. Moreau-Fauvarque C, et al. (2003) The transmembrane semaphorin Sema4D/CD100, an inhibitor of axonal growth, is expressed on oligodendrocytes and upregulated after CNS lesion. *J Neurosci* 23:9229–9239.
9. Low K, Culbertson M, Bradke F, Tessier-Lavigne M, Tuszynski MH (2008) Netrin-1 is a novel myelin-associated inhibitor to axon growth. *J Neurosci* 28:1099–1108.
10. Barrett CP, Guth L, Donati EJ, Krikorian JG (1981) Astroglial reaction in the gray matter lumbar segments after midthoracic transection of the adult rat spinal cord. *Exp Neurol* 73:365–377.
11. Bush TG, et al. (1999) Leukocyte infiltration, neuronal degeneration, and neurite outgrowth after ablation of scar-forming, reactive astrocytes in adult transgenic mice. *Neuron* 23:297–308.
12. Bradbury EJ, et al. (2002) Chondroitinase ABC promotes functional recovery after spinal cord injury. *Nature* 416:636–640.
13. Jones LL, Sajed D, Tuszynski MH (2003) Axonal regeneration through regions of chondroitin sulfate proteoglycan deposition after spinal cord injury: A balance of permissiveness and inhibition. *J Neurosci* 23:9276–9288.
14. McKeon RJ, Jurynec MJ, Buck CR (1999) The chondroitin sulfate proteoglycans neurocan and phosphacan are expressed by reactive astrocytes in the chronic CNS glial scar. *J Neurosci* 19:10778–10788.
15. Harel NY, Strittmatter SM (2006) Can regenerating axons recapitulate developmental guidance during recovery from spinal cord injury? *Nat Rev Neurosci* 7:603–616.
16. Wahl S, Barth H, Ciossek T, Aktories K, Mueller BK (2000) Ephrin-A5 induces collapse of growth cones by activating Rho and Rho kinase. *J Cell Biol* 149:263–270.
17. Kullander K, et al. (2001) Ephrin-B3 is the midline barrier that prevents corticospinal tract axons from recrossing, allowing for unilateral motor control. *Genes Dev* 15:877–888.
18. Miranda JD, et al. (1999) Induction of Eph B3 after spinal cord injury. *Exp Neurol* 156:218–222.
19. Willson CA, Miranda JD, Foster RD, Onifer SM, Whittemore SR (2003) Transection of the adult rat spinal cord upregulates EphB3 receptor and ligand expression. *Cell Transplant* 12:279–290.
20. Bundesen LQ, Scheel TA, Bregman BS, Kromer LF (2003) Ephrin-B2 and EphB2 regulation of astrocyte-meningeal fibroblast interactions in response to spinal cord lesions in adult rats. *J Neurosci* 23:7789–7800.
21. Benson MD, et al. (2005) Ephrin-B3 is a myelin-based inhibitor of neurite outgrowth. *Proc Natl Acad Sci USA* 102:10694–10699.
22. Goldshmit Y, Galea MP, Wise G, Bartlett PF, Turnley AM (2004) Axonal regeneration and lack of astrocytic gliosis in EphA4-deficient mice. *J Neurosci* 24:10064–10073.
23. Herrmann JE, Shah RR, Chan AF, Zheng B (2010) EphA4 deficient mice maintain astroglial-fibrotic scar formation after spinal cord injury. *Exp Neurol* 223:582–598.
24. Liu X, Hawkes E, Ishimaru T, Tran T, Sretavan DW (2006) EphB3: An endogenous mediator of adult axonal plasticity and regrowth after CNS injury. *J Neurosci* 26:3087–3101.
25. Leighton PA, et al. (2001) Defining brain wiring patterns and mechanisms through gene trapping in mice. *Nature* 410(6825):174–179.
26. Yokoyama N, et al. (2001) Forward signaling mediated by ephrin-B3 prevents contralateral corticospinal axons from recrossing the spinal cord midline. *Neuron* 29(1):85–97.
27. Kullander K, et al. (2003) Role of EphA4 and EphrinB3 in local neuronal circuits that control walking. *Science* 299:1889–1892.
28. Butt SJ, Lundfald L, Kiehn O (2005) EphA4 defines a class of excitatory locomotor-related interneurons. *Proc Natl Acad Sci USA* 102:14098–14103.
29. Egea J, et al. (2005) Regulation of EphA 4 kinase activity is required for a subset of axon guidance decisions suggesting a key role for receptor clustering in Eph function. *Neuron* 47:515–528.
30. Cafferty WB, Duffy P, Huebner E, Strittmatter SM (2010) MAG and OMgp synergize with Nogo-A to restrict axonal growth and neurological recovery after spinal cord trauma. *J Neurosci* 30:6825–6837.
31. Fischer D, He Z, Benowitz LI (2004) Counteracting the Nogo receptor enhances optic nerve regeneration if retinal ganglion cells are in an active growth state. *J Neurosci* 24:1646–1651.
32. Wang X, et al. (2011) Recovery from chronic spinal cord contusion after Nogo receptor intervention. *Ann Neurol* 70:805–821.
33. Templeton JP, et al. (2009) Differential response of C57BL/6J mouse and DBA/2J mouse to optic nerve crush. *BMC Neurosci* 10:90.
34. Perry VH, Morris RJ, Raisman G (1984) Is Thy-1 expressed only by ganglion cells and their axons in the retina and optic nerve? *J Neurocytol* 13:809–824.
35. Magnuson DS, et al. (2009) Swimming as a model of task-specific locomotor retraining after spinal cord injury in the rat. *Neurorehabil Neural Repair* 23:535–545.
36. Lemon RN (2008) Descending pathways in motor control. *Annu Rev Neurosci* 31:195–218.
37. Kim JE, Liu BP, Park JH, Strittmatter SM (2004) Nogo-66 receptor prevents raphespinal and rubrospinal axon regeneration and limits functional recovery from spinal cord injury. *Neuron* 44:439–451.
38. Mason P (2001) Contributions of the medullary raphe and ventromedial reticular region to pain modulation and other homeostatic functions. *Annu Rev Neurosci* 24:737–777.
39. Fujita Y, Endo S, Takai T, Yamashita T (2011) Myelin suppresses axon regeneration by PIR-B/SHP-mediated inhibition of Trk activity. *EMBO J* 30:1389–1401.
40. Chen C, et al. (2009) NgR RNA interference, combined with zymosan intravitreal injection, enhances optic nerve regeneration. *J Neurochem* 110:1628–1634.
41. Fu CT, Tran T, Sretavan D (2010) Axonal/glial upregulation of EphB/ephrin-B signaling in mouse experimental ocular hypertension. *Invest Ophthalmol Vis Sci* 51:991–1001.
42. Prestoz L, et al. (2004) Control of axonophilic migration of oligodendrocyte precursor cells by Eph-ephrin interaction. *Neuron Glia Biol* 1(1):73–83.
43. Petros TJ, Williams SE, Mason CA (2006) Temporal regulation of EphA4 in astroglia during murine retinal and optic nerve development. *Mol Cell Neurosci* 32(1-2):49–66.
44. Duffy P, et al. (2009) Rho-associated kinase II (ROCKII) limits axonal growth after trauma within the adult mouse spinal cord. *J Neurosci* 29:15266–15276.
45. Kim JE, Li S, GrandPré T, Qiu D, Strittmatter SM (2003) Axon regeneration in young adult mice lacking Nogo-A/B. *Neuron* 38(2):187–199.